Electronic supplementary Material (ESI) for Journal Materials Chemistry A.

Multifunctional glass fibre filter modified with vertical graphene for one-step dynamic water filtration and disinfection

Shuting Cheng,‡[ad] Mian Chen,‡[c] Kun Wang,‡[bd] Qingqing Liu,[d] Yi Cheng,[bd] Ruihua Dong,[c] Kewen Huang,[bd] Hao Yuan,[bd] Jun Jiang,[ad] Wenjuan Li,[bd] Junliang Li,[d] Ce Tu,[d] Jian Liu,[a] Xingyu Jiang,[c] Yue Qi,[bd] and Zhongfan Liu,*[bd]*

‡ These authors contributed equally to this work.

[a] State Key Laboratory of Heavy Oil Processing, College of Science, China university of Petroleum, No. 18, Fuxue Rd., Changping District, Beijing, 102249 P. R. China

[b] Centre for Nanochemistry, Beijing Science and Engineering Centre for Nanocarbons, Beijing National Laboratory for Molecular Sciences, College of Chemistry and Molecular Engineering, Peking University, No. 202, Chengfu Rd., Haidian District, Beijing, 100871 P. R. China

[c] Shenzhen Key Laboratory of Smart Healthcare Engineering, Department of Biomedical Engineering, Southern University of Science and Technology, No. 1088, Xueyuan Rd., Xili, Nanshan District, Shenzhen, Guangdong, 518055 P. R. China

[d] Beijing Graphene Institute (BGI), No. 13, Cuihunan Rd., Haidian District, Beijing, 100095 P. R. China

Email: Dr. Yue Qi, qiyue-cnc@pku.edu.cn

Prof. Zhongfan Liu, zfliu@pku.edu.cn;

Experimental section

Filters fabrication and characterization: GFF (TISSUQUARTZ-2500QAT-UP) was purchased from PALL Pallflex. Methane was chosen as the carbon source for both the growth of VG-GFF and HG-GFF. VG-GFF was prepared by PECVD at 600 °C with the radio frequency power of 180 W. HG-GFF was prepared by APCVD at 1050 °C for 2h. The morphology and detailed structure of VG-GFF was investigated by SEM (FEI Quattro S, acceleration voltage 5–10 kV), TEM (FEI Tecnai F20; acceleration voltage 200 kV), and Raman spectroscopy (Horiba, LabRAM HR 800, 532 nm laser wavelength). The thickness of graphene of HG-GFF was investigated by AFM (Bruker Dimension Icon with Tapping mode).

Electric field stimulation: The EF distribution was simulated by the finite element method. 3D models of VG-GFF and HG-GFF were set up respectively. For VG-GFF model, a graphene nanowall with the height of 1.49 μm and the length of 1 μm was constructed on the GFF surface with the length of 3 μm and the diameter of 1 μm to demonstrate the EF around the tip area. For HG-GFF model, graphene closely adheres to GFF in the circumferential and radial directions.

Purification performance analysis: E. *coli* (ATCC, 25922), S. *aureus* (ATCC, 29213), MDR E. *coli*, and MRSA (form local hospitals) were cultured within Luria-Bertani (LB) medium at a constant temperature incubator under shaking and then harvested by centrifugation at 8000 rpm. After washing with deionized (DI) water for 3 times, bacterial cells finally suspended in DI water to serve as the original bacterial suspension with a high concentration of ~10^7 colony-forming unit mL^{-1} (CFU mL^{-1}). The peristaltic pump (PHD ULTRA, Harvard Apparatus) was connected to the device to control the filtration flow rate

at a constant speed (2000 L h^{-1} m^{-2}). To study the EF disinfection performances, a power supply (RIGOL DG1062Z) through the pulse mode (1 kHz) was used to apply voltage (0 V, 3 V,5 V, 10 V) to contribute EF between two filters. And for the EH disinfection device, a DC power supply (TOMMENS TM-3010) was used to apply a voltage of 10 V. After flowing through the purification device, the bacterial solution was collected and their concentrations were characterized by plate counting method. The bacteria liquid has been diluted to a certain extent to prevent the bacteria from becoming too dense and affecting the counting. The removal efficiency was analysed according to the following equation[1]:

$$Efficiency = -log_{10}(C/C_0) \quad (1)$$

Where C and C_0 are the concentrations of the collected bacterial suspension after filtration and the original bacterial suspension.

Observation of bacterial viability: The fluorescent images of bacteria were collected by NIKON (A1R) confocal laser microscope for detecting bacterial viability. The bacteria with corresponding treatment were gathered through centrifugation (8000 rpm, 3 min) after several rinses with phosphate buffer saline（PBS) to remove LB medium and then stained with propidium iodide (PI) and SYTO 9 for 30 min in a dark place. Before observing by microscopes, the bacterial suspension was washed with PBS for reducing the unessential influence of dye.

SEM characterization of bacterial morphologies: After conducting the bactericidal assay, the experimental GFFs with bacteria absorbed were fixed with stationary liquid (2.5% glutaraldehyde) overnight at 4 °C. The treated bacterial samples were sequentially dehydrated with the increasing content of ethanol-water solution (30%, 50%, 75%, 90%,

and 100%) for 20 min for SEM characterization (Hitachi-SU8220). The dehydrated experiments should be careful to reduce superfluous damages on bacterial morphologies.

Measurement of membrane potential: The original bacterial suspension was exposed to DiSC3(5) dye for 30 min in a 37 °C cell incubator. The bacterial suspensions were centrifuged at 8000 rpm for 3 min after sequentially several rinses with PBS. The following bactericidal assays in the filter were the same as the previous procedure. The treated bacteria were collected by centrifugation and re-dispersed in 0.5 mL of PBS, and then the fluorescence intensity of PI at 622 nm excitation and 670 nm emission was recorded.

Measurement of membrane permeability: After flowing through the purification device, the bacteria were collected by centrifugation (8000 rpm, 3 min) and rinsed by PBS for 3 times. The treated bacteria were incubated in a 37 °C cell incubator for 30 min after adding with PI dye (10 μg mL^{-1}), then centrifuged and re-dispersed in 0.5 mL of PBS. Finally, the fluorescent intensity of PI at 488 nm excitation and 535 nm emission was recorded.

Evaluation of ATP level: The ATP level in bacteria was determined by using an ATP assay kit (Beyotime Biotechnology). After flowing through the purification device, the treated bacteria were collected by centrifugation (8000 rpm, 3 min) and rinsed by PBS for 3 times. The ATP level was evaluated according to the manufacturer's instructions.

Determination of intracellular ROS: The intracellular ROS level were analysed by ROS assay kit (S0033S, Beyotime Biotechnology) with fluorescent probe (DCFH-DA). The bacteria in the filter passing through the experimental filters were collected in DI water. DCFH-DA was diluted with PBS to a final concentration of 10 μmol mL^{-1}, and the centrifuged bacteria were incubated in a 37 °C cell incubator for 20 minutes. The bacteria treated with 0.1 mM H_2O_2 for 60 min was as a ROS-positive group. The fluorescent in each

hole at 488 nm excitation and 520 nm emission was recorded by a microplate reader (TECAN Spark, Switzerland).

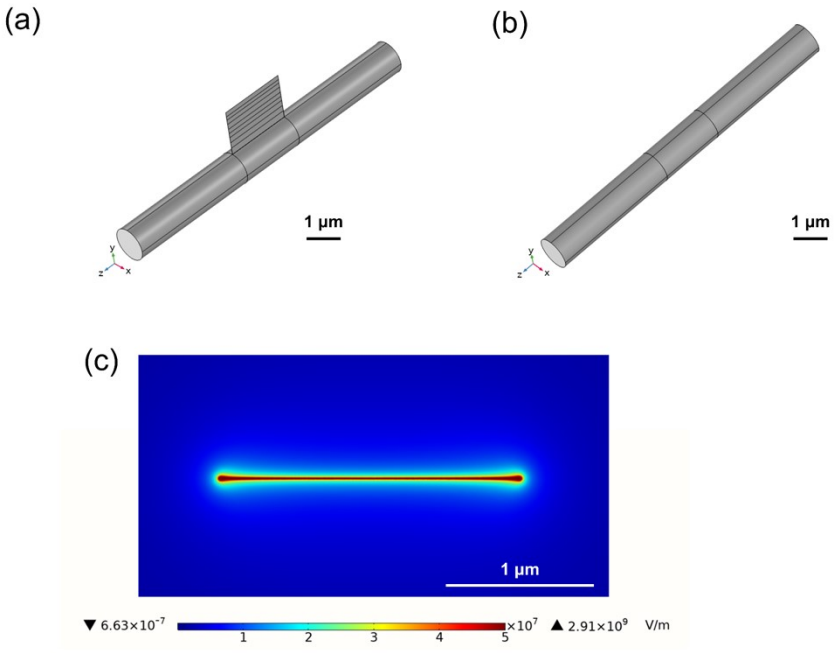

Figure S1. Simulation of EF distribution near the surface of GFF. (a,b) The 3D electrode models of VG-GFF (a) and HG-GFF (b). (c) Top view of the simulated EF around VG, showing the significantly enhancement of the localized EF near the sharp edge of VG.

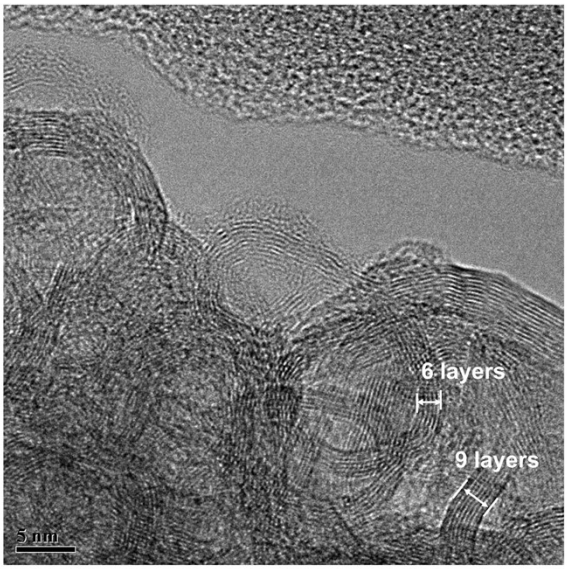

Figure S2. TEM image of VG on GFF after 1 h growth. Graphene thickness at the bottom of VG nanowalls is about 6−10 layers.

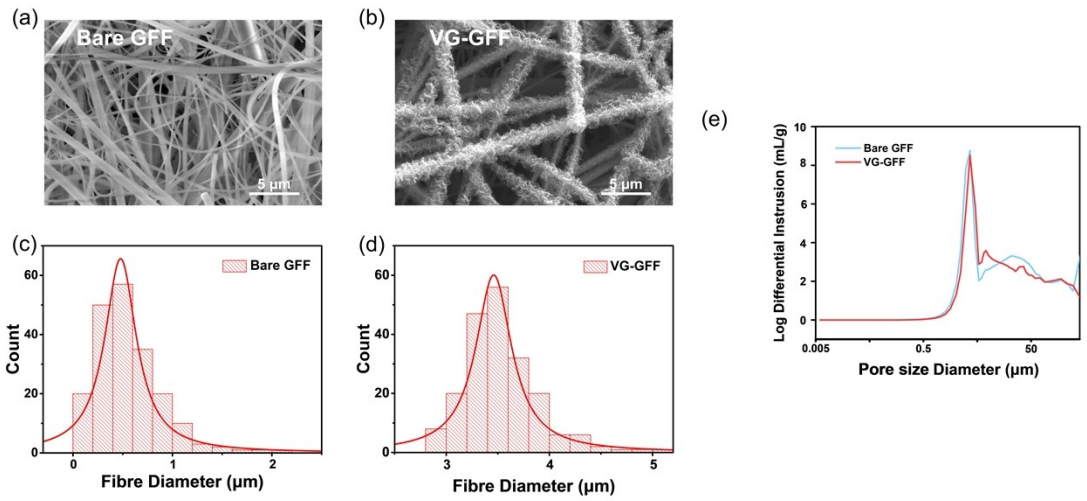

Figure S3. Diameter distributions of the fibre in bare GFF and VG-GFF samples. (a,b) Representative SEM images of bare GFF (a) and VG-GFF (b). (c,d) Statistic fibre diameter distributions of bare GFF (c) and VG-GFF (d). The average fibre diameter of the bare GFF was 0.55 μm. After modified with VG, the average diameter of the fibre increased to 3.54 μm. The statistics were obtained from 5 pieces of membranes and 40 different positions on each membrane. (e) Pore size distributions of bare GFF and VG-GFF. The average pore diameters of bare GFF and VG-GFF are 7.82 μm and 7.35 μm, respectively.

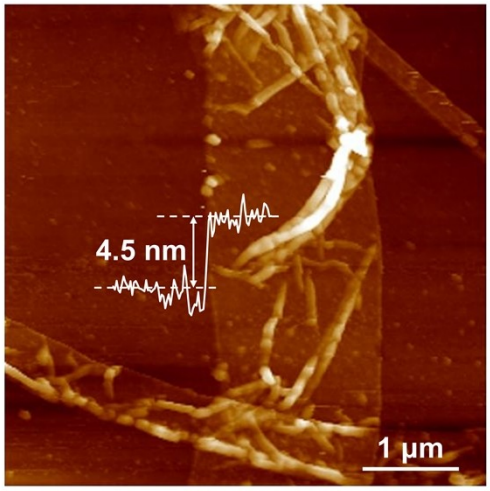

Figure S4. AFM image of graphene ribbon after etching the inner glass fibre of HG-GFF. The thickness of the obtained graphene ribbon is 4.5 nm, corresponding to the HG thickness of 2.25 nm and graphene layer number of 4-5.

After the core glass fibre was etched, the graphene shell was collapsed into a micro ribbon and the graphene covered above and below the glass fibre overlapped. Therefore, the height of the collapsed graphene ribbon is twice the thickness of HG. The layer of graphene is calculated based on 0.5 nm per graphene layer.[2]

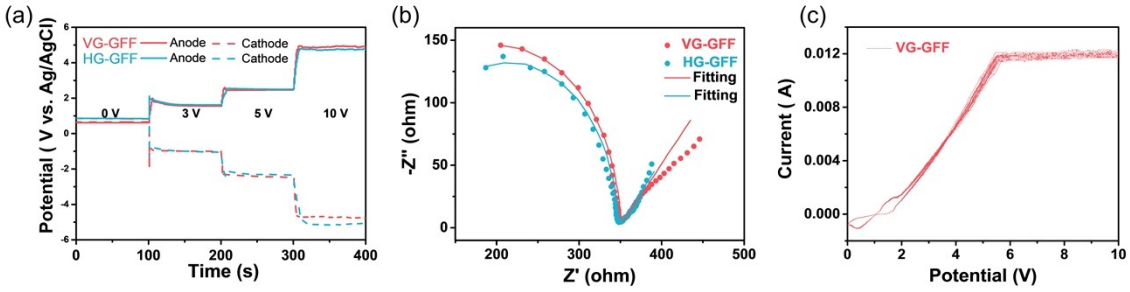

Figure S5. Electrochemical properties of VG-GFF and HG-GFF. (a) Cathode and anode potentials in V vs Ag/AgCl of VG-GFF and HG-GFF, which was electrolyzed at 0-10 V. (b) Nyquist plots of EIS spectra of VG-GFF and HG-HGG. The inset is the equivalent circuit diagram. (c) CV plot of 50-cycles from 0 to10 V of VG-GFF.

Electrochemical measurements were performed in 10 mM NaCl solution at room temperature using a CHI760C electrochemical workstation and an electrochemical cell with three electrodes (VG-GFF and HG-GFF samples functioning as the working electrodes with the exposed area of 1 cm * 1 cm, platinum tablets functioning as the counter electrode, and Ag/AgCl electrode as the reference electrode). As shown in Fig. S5a, the cathode-anode potentials of VG-GFF and HG-GFF at different voltages are similar, indicating that the electrical conductivity of VG-GFF and HG-GFF showed negligible difference. Then, EIS was performed to analyze the conductive properties at the anode OCP at 10 V. The value of the membrane resistance can be roughly judged from the radius of the arc in the Nyquist spectra, and the specific numerical value of the membrane resistance can be obtained by fitting the equivalent circuit. As shown in Fig. S4b, circuit fitting results of VG-GFF and HG-GFF revealed that the membrane resistances (R) of VG-GFF and HG-GFF are 291.1 ohm cm^{-2} and 264.3 ohm cm^{-2}, respectively. Further, the electrical conductivity (σ) of membrane can be calculated according to the formula:

$$\sigma = 1/Rw \qquad (1)$$

where *w* is membrane thickness. The w of VG-GFF and HG-GFF is 432 μm, and thus the calculated σ is 7.94 S m^{-1} and 8.77 S m^{-1}, respectively. From the measured results of the cathode-anode potential, membrane resistance, and conductivity, HG-GFF and VG-GFF showed negligible difference in conductivity.

CV test at a scan rate of 50 mV s^{-1} was used to evaluate the long-term stability of VG-GFF. As shown in Fig. S4c, the current at 10 V drops by only 0.0002 A (from 0.0119 A to 0.0117 A) after 50 cycles (about 6 h), indicating the good stability of VG-GFF.

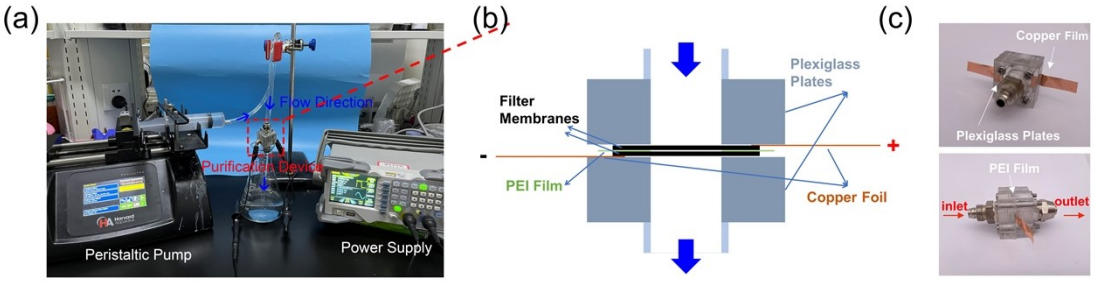

Figure S6. Design of the purification system. (a) Photograph of the experiment setup. The original bacterial liquid pumped by peristaltic pump flows through the purification filter and reaches the collection bottle. (b,c) Photographs (b) and schematic diagram (c) of the purification filter. Two parallel filter membranes are separated by PEI film and connected with two copper foil electrodes, for the power supply.

In the design, the filter part was constructed with two 3 cm × 3 cm × 1 cm plexiglass plates with a cylindrical hole (the area of 1cm^2) in the centre. The two prepared filter membranes were placed in parallel between plexiglass plates and separated by a 200-μm PEI film. Two pieces of copper foil were used to connect the two parallel filter membranes for the power supply (Fig. S6b). Notably, to ensure the flatness of the sample surface and the tight connection between the electrodes, the whole device was fixed and clamped tightly by the surrounding screws (Fig. S6c). Then the flowing rate of bacterial suspension was precisely controlled by the peristaltic pump to guarantee the same number of bacteria flowing through the unit area of the filter with the same retention time. Meanwhile, the voltage applied to the parallel filter was precisely controlled by a digital power supply to ensure the stability of the local EF. With the above elaborate designs of the purification

apparatus, the uniformity of the system and the reliability of results were well guaranteed irrespective of the size of the sample.

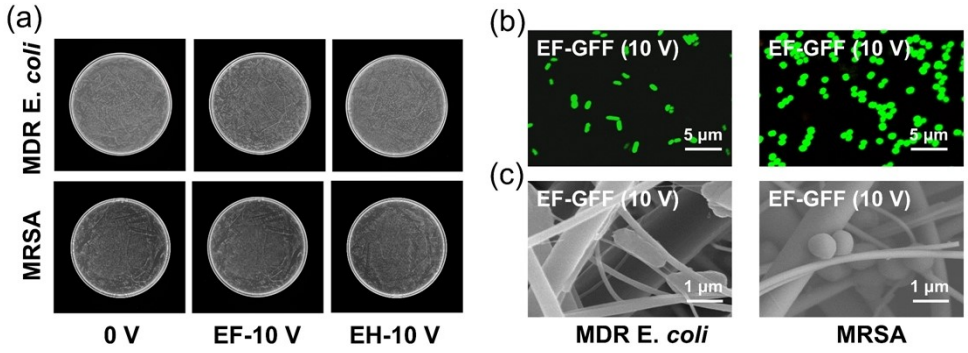

Figure S7. Purification performances of bare GFF device as control. (a) Plating results of MDR E. *coli* and MRSA in the filtrate after flowing through bare GFF at 0 V, EF-10 V and EH-10 V. (b) Live/dead fluorescent staining of MDR E. *coli* and MRSA in the filtrate. (c) Representative SEM images of MDR E. *coli* and MRSA on bare GFF after filtration and disinfection. After filtration, the bacteria remain viability and the cell membrane maintain smooth, indicating that GFF only physically intercepts the bacteria instead of physiological inactivation. Error bars represent the standard deviation calculated from three replicates from three different preparation batches (each replicate consists of a pair of filter membranes from the same batch).

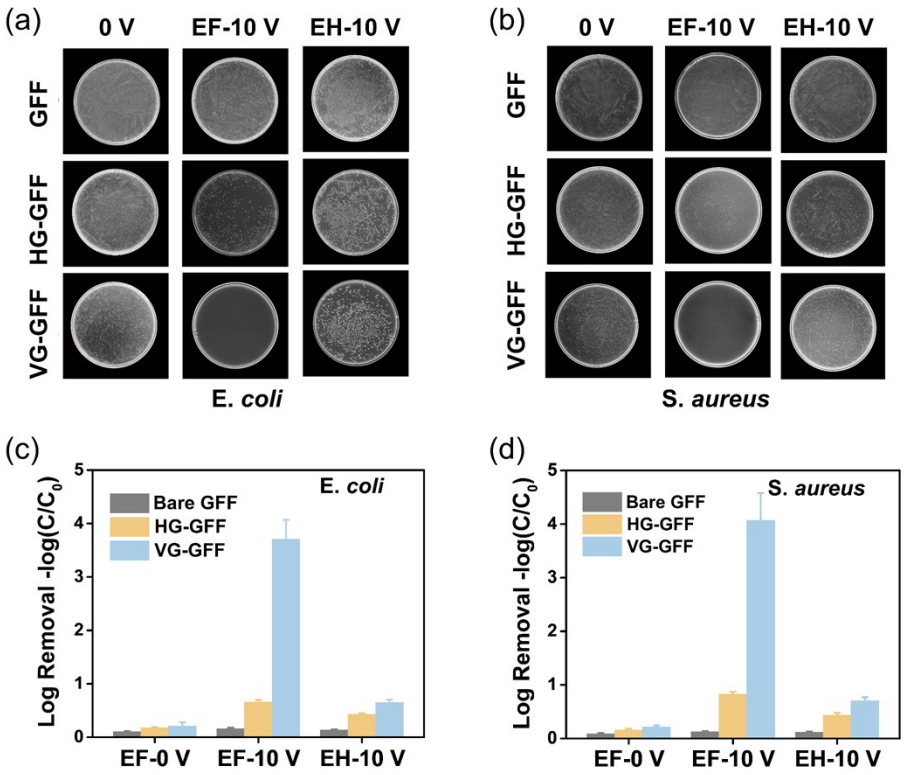

Figure S8. Purification performances of EF-VG-GFF devices for E. *coli* and S. *aureus*. (a,b) Plating results of E. *coli* (a) and S. *aureus* (b) in the filtrate after being purified with different approaches. (c, d) Corresponding statistics of E. *coli* (c) and S. *aureus* (d) from the samples in (a,b). EF-VG-GFF (10 V) achieved the best purification performances with >3.7 and >4.0 log removal efficiency for E. *coli* and S. *aureus*, respectively. Error bars represent the standard deviation calculated from three replicates from three different preparation batches (each replicate consists of a pair of filter membranes from the same batch).

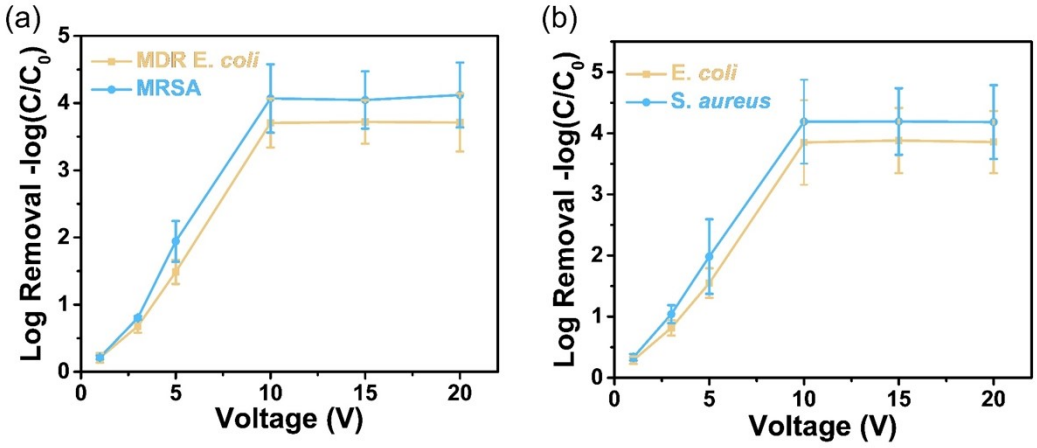

Figure S9. Purification performances of EF-VG-GFF for examined bacteria at different applied voltages. (a,b) Purification performances of EF-VG-GFF for MDR bacteria (a), and E. *coli* and S. *aureus* (b) at different applied voltages (1, 3, 5, 10, 15 and 20 V). Error bars represent the standard deviation calculated from three replicates from three different preparation batches (each replicate consists of a pair of filter membranes from the same batch).

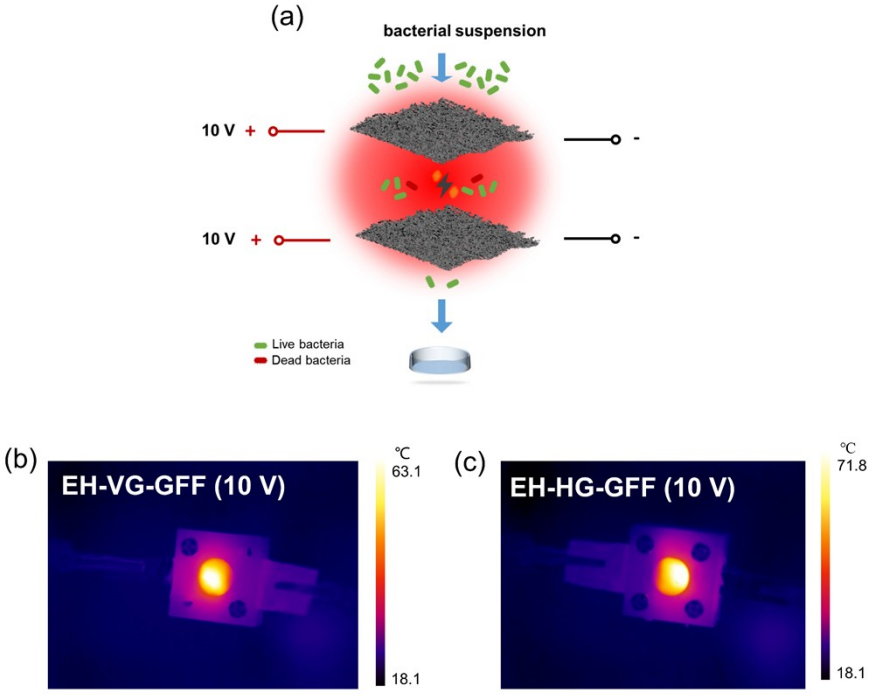

Figure S10. EH purification device based on VG-GFF. (a) Schematics of the EH purification device. (b,c) Temperature images captured by infrared camera of VG-GFF (b) and HG-GFF (c) at EH-10 V.

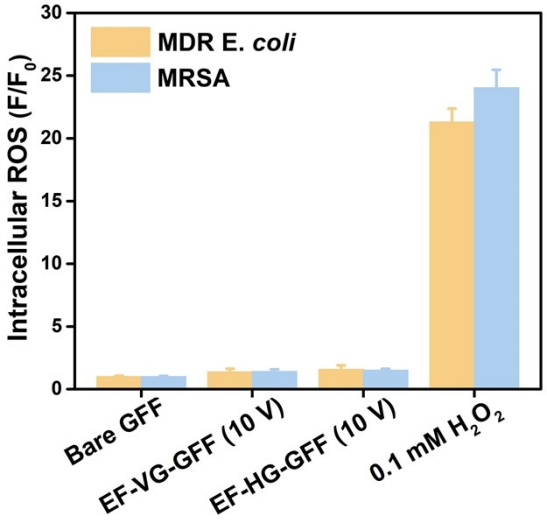

Figure S11. Measurement of the intracellular reactive oxygen species (ROS), indicating the tiny contribution of ROS to disinfection performance of EF-VG-GFF device.

Table S1. Retention time in EF disinfection process.

Flux [a] ($L\ h^{-1}\ m^{-2}$)	**h** [b] (Distance between two electrodes, μm)	**t** [c] (Retention time, s)
2000	200	0.36

[a] Flux = 2000 $L\ h^{-1}\ m^{-2} = 5.6 \times 10^{-4}\ m\ s^{-1}$

[b] h = 200 μm = 2×10^{-4} m

[c] t = h/Flux = 0.36 s

References

1 A. Li, Y. Zi, H. Guo, Z. L. Wang and F. M. Fernández, *Nat. Nanotechnol.* 2017, **12**, 481–487.

2 H. Yuan, H. Zhang, K. Huang, Y. Cheng, S. Cheng, W. Li, J. Jiang, C. Tu, X. Wang, Y. Qi and Z. Liu, *ACS Nano*, 2020, **16**, 2577–2584.